Available online at www.sciencedirect.com
SCIENCE DIRECT®
C. R. Physique 4 (2003) 175–186
COMPTES RENDUS PHYSIQUE

Optical telecommunications/Les télécommunications optiques

# Holey optical fibres: Fundamental properties and device applications

# Fibres microstructurées : propriétés fondamentales et applications du composant

Tanya M. Monro *, David J. Richardson

*Optoelectronics Research Centre, University of Southampton, SO17 1BJ, UK*

Received 26 November 2002

Presented by Guy Laval

**Abstract**

The presence of wavelength-scale holes in the transverse profile of a holey fibre can lead to novel optical properties that cannot be achieved in more conventional forms of optical fibre. Examples of such properties include broadband single-mode guidance, the extremes of fibre nonlinearity, from fibres providing tight mode confinement to those offering large mode areas, and a range of remarkable dispersive properties, including broadband flattened dispersion, anomalous dispersion below 1.3 μm, and large normal dispersion values at 1.55 μm. Fundamentals and recent progress are reviewed, ranging from design and fabrication through to applications and devices based on this emerging fibre type. ***To cite this article: T.M. Monro, D.J. Richardson, C. R. Physique 4 (2003).***



**Résumé**

La présence de trous à l'échelle de la longueur d'onde dans le plan transverse d'une fibre « éponge » peut produide des propriétés optiques nouvelles qu'on ne pourrait obtenir avec des fibres de formes plus conventionnelle. Les exemples de telles propriétés sont un guidage unimodal à bande large, des caractéristiques non-linéaires extrêmes telles qu'un fort confinement modal ou bien une grande aire modale effective, et un ensemble de propriétés dispersives remarquables telle qu'une dispersion aplatie large-bande, qu'une dispersion anormale en-dessous de 1,3 μm et que des dispersions normales à 1,55 μm. Nous passons en revue les aspects fondamentaux ainsi que les récents progrès effectués, de la conception et la fabrication aux applications et aux composants basés sur ce nouveau type de fibre. ***Pour citer cet article : T.M. Monro, D.J. Richardson, C. R. Physique 4 (2003).***



*Keywords:* Micro-structured optical fibres; Holey optical fibres; Photonic crystal fibres; Fibre design and fabrication; Nonlinear fibre devices

*Mots-clés :* Fibres optiques micro-structurées ; Fibres « éponge » ; Fibres à crystal photonique photonic ; Conception et fabrication (des fibres) ; Composants non-linéaires à fibre

* Corresponding author.
*E-mail address:* tmm@orc.soton.ac.uk (T.M. Monro).

1631-0705/03/$ – see front matter 
doi:10.1016/S1631-0705(03)00004-5

## 1. Introduction

The microstructured fibre is a new class of optical fibre that has emerged in recent years [1]. Microstructured fibres contain an arrangement of air holes that run along the fibre length, and examples are shown in Fig. 1. The holes within these fibres act as the fibre cladding, and light can be guided using either one of two quite different mechanisms.

*Index-guiding* microstructured fibres guide light due to the principle of modified total internal reflection, and such fibres are widely known as *holey fibres* (HFs). The holes act to lower the effective refractive index in the cladding region, and so light is confined to the solid core, which has a relatively higher index. Unlike conventional fibres, HFs can be made entirely from a single material, typically un-doped silica, although HFs have also been fabricated in chalcogenide glass [2] and in polymers [3]. The basic operation of index-guiding fibres does not depend on having a periodic array of holes [4]. However, in practice the holes are typically arranged on a hexagonal lattice, and so these fibres are sometimes referred to as *photonic crystal fibres*.

The effective refractive index of the cladding can vary strongly as a function of the wavelength of light guided by the fibre. For this reason, it is possible to design fibres with spectrally unique properties not possible in conventional optical fibres. In addition, the optical properties of index-guiding HFs are determined by the configuration of air holes used to form the cladding, and many different arrangements can be envisaged within this flexible fibre type. The dispersion and polarization properties of a HF can be particularly strongly influenced by the cladding configuration, particularly when the hole-to-hole spacing is small. Simply by scaling the dimensions of the features within the fibre profile, HFs can have mode areas ranging over three orders of magnitude [5]. Fibres providing tight mode confinement can be used as the basis for devices based on nonlinear effects [6], whereas large mode fibres allow high power operation [7]. In addition, these fibres can exhibit properties not readily attainable in conventional fibres, including broadband single-mode guidance [8] and anomalous dispersion at wavelengths down to 550 nm [9].

Microstructured optical fibres can guide light by an alternative guidance mechanism if the air holes that define the cladding region are arranged on a periodic lattice. Periodic cladding structures can exhibit photonic bandgaps, and frequencies located within the bandgap cannot propagate within the cladding [1,10]. By breaking the periodicity of the cladding (e.g., by adding an extra hole to form a low-index defect), it is possible to introduce a localized mode within this defect. Such a defect can act as the core, and guide light within well-defined frequency windows. These *photonic bandgap fibres* can be designed to have transmission windows centred at near-infrared wavelengths [11].

The first index-guiding holey fibre was fabricated in 1996 [12], and since then progress in this field has been rapid. Holey fibres have matured into a technology with the potential to revolutionize many areas in communications and beyond. Here we aim to provide an overview of the properties and applications of this emerging fibre type.

## 2. Holey fibre design and fabrication

The vast majority of silica holey fibres produced to date have been fabricated using stacking techniques. Capillary tubes are stacked in a hexagonal configuration, and the central capillary can then be replaced with a solid silica rod, which ultimately forms the fibre core. This preform is then reduced in scale on a fibre drawing tower. This can either be done in a single step, or, if small-scale features are required in the final fibre, two scale reduction stages can be used. The parameters that characterise a HF profile are the hole-to-hole spacing $\Lambda$, the hole diameter $d$ and the number of rings of holes used to define the cladding region. The stacking procedure is a flexible one: holey fibres suitable for active devices can be made using a doped core rod, and multi-core fibres can be produced by introducing multiple rods into the stack.

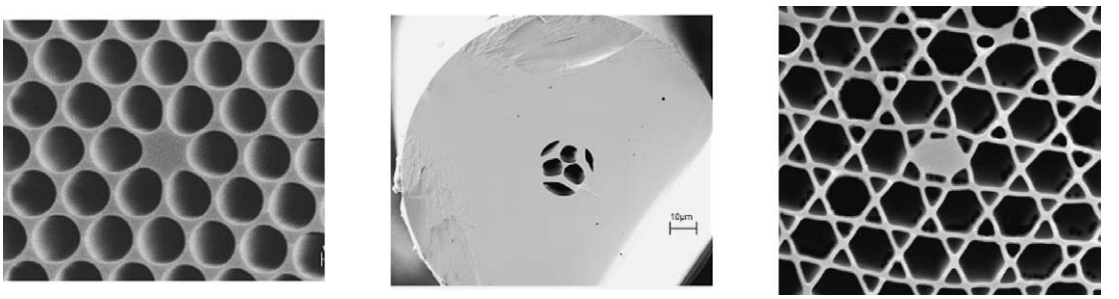


Fig. 1. SEM photographs of some typical small core holey optical fibres. Left: 1.2 μm-core pure-silica HF. Centre: HF produced when the Schott lead glass SF57 is extruded to form the fibre preform (core diameter 2 μm). Right: $Yb^{3+}$-doped HF with $2.6 \times 1.5$ μm elliptical core.

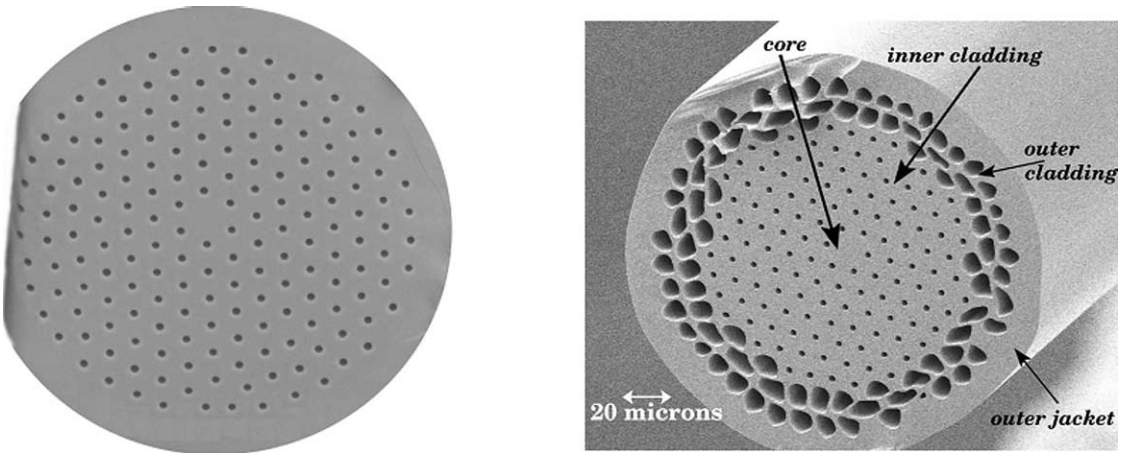


Fig. 2. SEM photographs of large mode area holey fibres (LMHFs). Left: Silica LMHF with a 15 μm core. Right: $Yb^{3+}$-doped silica double clad LMHF.

Although stacking is the principal technique that has been used to make holey fibres preforms thus far, other techniques have recently been demonstrated. Silica holey fibres have been made using sol–gel casting techniques [13], and the preform can be extruded directly from bulk glass using glasses with low-softening temperatures [14]. Extrusion offers the prospect of fibre designs that could not be envisaged with stacking techniques (and vice versa). Stacking techniques were used to make all fibres shown in Figs. 1 and 2 except Fig. 1 (centre), which was produced using extrusion.

The presence of wavelength-scale holes in HFs leads to a number of challenges in the accurate modelling of their optical properties. The complexity of the transverse refractive index profile generally precludes the direct use of analysis methods from traditional fibre theory. However, some insight into the operation of HFs can be obtained using a simple scalar effective index model [8], which replaces the holey cladding with a uniform material with the same effective refractive index. At any given wavelength, this effective index is obtained by solving the scalar wave equation in a hexagonal cell centred on a single hole. The properties of the fibre can then be estimated by evaluating the properties of the equivalent step-index fibre, using the calculated (strongly wavelength dependent) effective cladding index. It is this strongly wavelength-dependent cladding index that leads to many of the novel properties of holey fibres. The effective index method correctly predicts the endlessly single-mode guidance regime in small-hole HFs (for which $d/\Lambda < 0.4$). However this reduced model cannot accurately predict properties such as dispersion or birefringence that are sensitive to the cladding geometry. In addition, to date no satisfactory method for ascribing parameters to the equivalent fibre has been found that works for all designs and wavelengths [15], and it is in general necessary to make reference to the results of full numerical models.

Hence, in order to accurately model HFs it is typically necessary to account for the complex spatial distribution of air holes that define the cladding, and here a range of techniques are outlined. Many of these techniques have been successfully applied to both to index-guiding and bandgap fibres. In general, a combination of techniques is required to obtain a complete picture of the properties of any given microstructured fibre. Note that when the effective index contrast between core and cladding is large ($d/\Lambda > 0.5$), the weak-guidance (scalar) approximation breaks down, and it is often necessary to adopt a vectorial method.

*Beam propagation methods* (BPM) can also be used to calculate the properties of HFs [16], as can the finite element method [17]. In the finite element method, the fibre profile is partitioned into distinct homogeneous subspaces. By solving discretized Maxwell equations for each element, and imposing continuity conditions on the element boundaries, it is possible to calculate the modal fields of an arbitrary HF structure. Both of these techniques are relatively inefficient computationally.

The *plane wave method* [18] describes the magnetic field as a plane wave decomposition. To incorporate the core, it is necessary to create a supercell including the core that is then periodically repeated. This approach is also computationally intensive since many plane waves are required for an accurate description. An alternative approach exploits the localisation of the mode in the core, and so is more efficient than the plane-wave methods [5,19]. Both techniques can be used to predict the properties of arbitrary HF profiles.

Most of the modelling performed to date has considered periodic hexagonal arrangements of air holes. Group theory arguments can be used to show that all symmetric structures with higher than 2-fold symmetry do not exhibit form birefringence [20]. However, as the techniques described thus far are based on a Cartesian grid, they typically predict a small degree of birefringence that can be reduced (but not eliminated) by using a finer grid. However, when modelling asymmetric structures with a form birefringence that is significantly larger than this false birefringence, it is possible to make useful predictions.

The modes of single-material HFs are leaky because the core refractive index is the same as that beyond the finite holey cladding, and for some designs, this can lead to significant confinement loss [21]. It is always possible to reduce the confinement loss by increasing the distance between the core and the region beyond the cladding region: for a stacked HF, this can be done by adding more rings of holes. Apart from the BPM approach, none of the techniques described above can calculate complex propagation constants.

The *multipole approach* [21] can be used to explore effects introduced by the finite nature of the cladding because it does not use periodic boundary conditions. Another advantage of this method is that it avoids the false birefringence described above. However, the multipole approach is restricted to circular or at most elliptical inclusions, and so cannot be applied to HFs with arbitrary cladding configurations.

Finally, another technique that is capable of predicting confinement loss is based on representing the index distribution in terms of annular segments [22]. The algorithm uses a polar coordinate-based Fourier decomposition method with adjustable boundary conditions to model the outward radiating fields. This approach is particularly well suited to structures like the one in Fig. 1 (centre) with a limited number of cladding features.

## 3. Nonlinear holey fibres

One particularly promising application of holey fibre technology is in the development of fibre devices based on nonlinear optical effects [6]. Nonlinear effects can be used for a wide range of optical processing applications including optical data regeneration, wavelength conversion, optical demultiplexing, and Raman amplification. There is great interest in the development of fibres with high values of effective nonlinearity per unit length, and here we review the optical properties of these small-core fibre designs, and in Section 6, some of the emerging device applications of this new class of fibres are described.

A measure of fibre nonlinearity is the effective nonlinearity $\gamma$ [23]: $\gamma = 2\pi n_2/(\lambda A_{\text{eff}})$, where $n_2$ is the nonlinear coefficient of the material, $\lambda$ the wavelength and $A_{\text{eff}}$ is the effective mode area. Even though silica is not a particularly nonlinear material ($n_2 \approx 2.2 \times 10^{-20}$ m$^2$/W), the nonlinear properties of silica optical fibres can be utilized when high light intensities are guided. Conventional Corning SMF28 fibre has $\gamma \approx 1$ W$^{-1}\cdot$km$^{-1}$ at 1550 nm. By reducing the core diameter (reducing $A_{\text{eff}}$), and using high germanium concentrations within the core (which both enhances $n_2$ and improves the confinement of light) values of $\gamma$ as large as 20 W$^{-1}\cdot$km$^{-1}$ have been achieved in conventional fibres [24].

Holey fibres can have a significantly larger NA than solid fibres because the cladding can be mostly comprised of air when the air-filling fraction is large (i.e., large $d/\Lambda$), and so light is confined more tightly within the core. When large air-filling fractions are used in combination with wavelength-scale cladding features, small mode areas large values of $\gamma$ result. One example of such a highly nonlinear silica holey fibre is shown in Fig. 1 (left). Effective fibre nonlinearities of more than $\gamma \sim 60$ W$^{-1}\cdot$km$^{-1}$ at 1550 nm have been measured in pure silica holey fibres [25]. Hence, it is possible to achieve fibre nonlinearities more than 50 times higher than in standard telecommunications fibre.

Fibre losses less than 1 dB/km have now been demonstrated in pure silica index-guiding HFs at 1550 nm [26]. However, reducing the core diameter to dimensions comparable to the wavelength of light generally increases the fibre loss. This occurs for two principal reasons: in such fibres, the light interacts much more with the air/glass boundaries near the core, and so the effect of surface roughness becomes significant [26], and unless many rings of holes are used, the mode can *see over* the finite cladding region, and so confinement loss can have a significant impact [27].

Unsurprisingly, lower confinement loss and tighter mode confinement can always be achieved by using fibres with larger air-filling fractions. However, even using a large air-filling fraction, in the limit that the core dimensions are smaller than the wavelength of light guided by the fibre, more than 6 rings of air holes are required to ensure low-loss operation. In general, it is not always desirable to use the structures that offer the smallest values of effective mode area. A modest increase in the structure scale in this small core regime can lead to dramatic improvements in the confinement of the mode without compromising the achievable effective nonlinearity significantly. With careful design, it is possible to envisage practical HFs with small core areas ($<2$ μm$^2$) and low confinement loss ($<0.2$ dB/km). Note that although fibre loss limits the effective length of any nonlinear device, for highly nonlinear fibres, short lengths ($<10$ m) are typically required, and so loss values of order of 1 dB/km can be readily tolerated.

Highly nonlinear HFs can exhibit a range of novel dispersive properties [5]. Modifications of the fibre design allow the magnitude, sign and slope of the dispersion to be tailored to suit a range of device applications. HFs can exhibit anomalous dispersion down to 550 nm [9], which has made soliton generation and propagation in the near-IR and visible spectrum possible. An application of this regime was reported in [28], in which the soliton self-frequency shift was used as the basis for a femtosecond pulse source tunable from 1.06–1.33 μm. Shifting the zero-dispersion wavelength to regimes where there are convenient sources also allows the development of efficient super-continuum sources [29], which are attractive for DWDM transmitters, pulse compression and the definition of precise frequency standards. It is also possible to design nonlinear HFs

with normal dispersion at 1550 nm [30]. Fibres with low values of normal dispersion are advantageous for optical thresholding devices, since normal dispersion reduces the impact of coherence degradation [31] in a nonlinear fibre device, whereas fibres with high values of normal dispersion may have application in dispersion compensation.

The combination of wavelength-scale features and a large refractive index contrast can lead to large form birefringence effects in this fibre type. For example, consider the fibre in Fig. 1 (right), which has an elliptical core. The measured beat length for this fibre is just 0.3 mm at 1550 nm, and the polarization extinction ratio is 18 dB. Indeed, even small asymmetries can led to noticeable birefringence in small-core fibre designs.

Moving to high refractive index glasses, it is possible to access significantly larger material nonlinearities. For example, the chalcogenide glass $As_2S_3$ is 100 times more nonlinear than silica ($n \approx 2.4$ @ 1550 nm, $n_2 \approx 2 \times 10^{-18}$ m$^2$ W$^{-1}$) [32] and the Schott lead-glass SF57 is 20 times more nonlinear than silica ($n \approx 1.8$ @ 1550 nm, $n_2 \approx 4 \times 10^{-19}$ m$^2$ W$^{-1}$ [33]). Although compound glasses are clearly attractive for nonlinear devices, their application has been limited because it has proved difficult to produce conventional solid fibres that are single-mode and low-loss in these materials.

The combination of HF technology and compound glass is attractive for a number of reasons. Single-material fibre designs avoid core/cladding interface problems, and so should ultimately allow fibres to be drawn from a wide range of glasses. Also, compound glasses generally have significantly lower softening temperatures than silica, and so are amenable to a broader range of HF preform fabrication techniques (see Section 3). In addition, HFs offer extremely high fibre nonlinearity through the combination of a large material $n_2$ with tight mode confinement. This was demonstrated for the SF57 fibre pictured in Fig. 1 (centre), which represents the first demonstration of single-mode guidance in a non-silica HF [14]. The effective nonlinearity of this fibre was measured to be $\gamma \approx 550$ W$^{-1}$·km$^{-1}$ at 1550 nm, more than 500 times more nonlinear than standard optical fibre. There is scope for further enhancements in fibre nonlinearity by moving to more nonlinear glasses and/or using fibre designs offering tighter mode confinement. Such fibres promise a route towards nonlinear fibre devices with unprecedentedly low operating powers (10–100 mW) and remarkably short device lengths (0.1–1 m).

## 4. Large mode area holey fibres

Large mode area fibres are important for a wide range of applications most notably the delivery of high power optical beams. Relatively large mode area single-mode fibres can be made using conventional fibre doping techniques such as modified chemical vapour deposition by reducing the numerical aperture (NA) and increasing the diameter of the fibre core. However, the minimum NA that can be achieved is restricted by the accuracy with which the index difference between the core and cladding can be controlled.

Holey fibres offer an attractive alternative route towards fibres with large mode areas [7]. HF technology also provides a potentially more accurate route to controlling the index difference between core and cladding regions. Large mode area holey fibres (LMHFs) can be produced either by using a large hole-to-hole spacing ($\Lambda > 5$ μm) and/or a small air-filling fraction ($d/\Lambda < 0.3$). Single mode HFs with mode areas as large as 680 μm$^2$ at 1550 nm have been produced [34], and Fig. 2 (left) shows an SEM of a pure silica LMHF. In addition to offering large mode areas, LMHFs can be single-moded at all wavelengths. This is in contrast to standard optical fibres, which exhibit a cut-off wavelength below which the standard fibre becomes multi-moded.

As for conventional fibre designs, macroscopic bend loss ultimately limits the mode area scaling that can be utilized in these fibres. In conventional solid fibres, bend loss increases at long wavelengths, because the fibre becomes more weakly guiding, and thus is more susceptible to bend loss. In addition to this long wavelength bend loss edge, HFs possess a bend loss edge at short wavelengths [7]. In essence, light can also escape from the bent fibre by leaking between the cladding holes. Unsurprisingly, the critical bending radius below which catastrophic bend loss occurs, and the spectral width and location of the operational window between the short and long-wavelength bend loss edges are determined by the cladding geometry. Hence, to design practical LMHFs, it is crucial to have methods for estimating the impact of the fibre design on the fibre bend loss.

Previous work on conventional fibres has identified two distinct bend loss mechanisms; transition loss and pure bend loss [35]. As light travels into a curved fibre, the mode distorts, causing a transition loss (analogous to a splice loss) between straight and curved fibre sections. Pure bend loss occurs continually along any curved section of fibre: the tails of the mode cannot travel fast enough to negotiate the bend, and are thus lost. The results described above have focussed on pure bend losses, which are the dominant form of bend loss in long fibre lengths. However, for shorter lengths of fibre, or for fibres containing microbends, the impact of transition loss can also be significant.

Using the effective index method described in Section 3, it is possible to estimate the pure bend losses by applying standard results for step-index fibres. This method predicts that larger holes (i.e., larger $d/\Lambda$) result in broader operational windows, whereas the hole-to-hole spacing $\Lambda$ roughly determines the centre position of the operational window: minimum bend losses occur for wavelengths near $\Lambda/2$ [36]. Although telecommunications wavelengths fall on the short wavelength edge for LMHF designs, which generally have $\Lambda > 5$ μm, experiments show that LMHFs typically exhibit comparable bending losses to similarly sized conventional fibres at 1550 nm [34].

Although effective index methods can provide some useful bend loss estimates, to obtain a full description of the bend loss characteristics of LMHFs, it is necessary to account for the complex cladding configuration. For example, measurements indicate that the orientation of the bend in the fibre relative to the holes can have a noticeable effect on the bend loss characteristics [37].

The propagation of light in a fibre with a radius of curvature $R_0$ can be modelled by scaling the transverse refractive index profile via: $(1 + (2r\cos\alpha)/R_0)^{1/2}$, where the coordinates are defined in [38]. By applying this transformation to the complex HF cladding geometry the modes of the bent fibre can be calculated directly. Using these modes, both transition and pure bend losses can be predicted. This approach allows trends relating to the details of the cladding geometry and angular orientation of the fibre to be identified [37].

## 5. Device applications

As described in Section 4, HFs can have high values of nonlinearity per unit length and thus nonlinear optical devices based on holey fibre can be much shorter in length, and/or operate at lower power levels than devices based on conventional fibre types. Holey fibres thus promise practical nonlinear fibre devices for use within a variety of application areas including future high capacity optical communication systems. To date most HF communication device work has concentrated on the use of small core silica HFs, which have around 50 times the nonlinearity of standard fibres. This reduces the typical power length product requirements of such devices to the 10 W·m level. The development of compound glass holy fibres should ultimately allow sub-metre/sub-Watt devices to be realised. In this section we review a selection of holey fibre device demonstrators that highlight some of the key features of nonlinear holey fibres. These early demonstrators give insight into the device possibilities and performance that can ultimately be expected with further improvements in this exciting technology.

The first true demonstration of the use of holey fibre to perform a function required within telecommunications was reported in 2001 and concerned $2R$-optical regeneration and optical thresholding [39]. The regeneration technique employed had previously been demonstrated using conventional fibres by Mamyshev [40] and makes use of spectral broadening of a pulse due to *self-phase modulation* (SPM). The HF that was used for this demonstration is shown in Fig. 3(a). A filter is set with its peak transmission wavelength offset from the central wavelength of an incoming data stream such that low power pulses propagating within the HF generate little SPM and are thus largely rejected by the filter. By contrast higher power pulses generate appreciable SPM (see Fig. 3(b)) such that significant power is now generated at wavelengths within the filter passband. These spectral components are then transmitted by the filter. It can be shown that around some critical input pulse intensity $I_i$ the intensity of the output pulses $I_0$ becomes independent of $I_i$, providing $I_i$ is large enough to produce sufficient SPM. Such a nonlinear response can be used as a means to provide $2R$ regeneration since 'noisy' zero bits are suppressed and noisy 'one' bits have their intensities equalized. The reshaping part of the $2R$ process is obtained through the narrowband filtering process itself assuming that a filter with an appropriate phase and amplitude response matched to the incoming pulse response is used. A plot of a typical nonlinear transmission response for such a switch is shown in Fig. 3(c). The S-shaped transmission characteristic is just as required for $2R$-regeneration and optical thresholding applications. In this particular instance the length of holey fibre used was 8.7 m, and the operating switching power was $\sim$2 W. This particular switch was used as an optical thresholder within an Optical Division Multiple Access (OCDMA) receiver and allowed error-free performance with reduced power penalty relative to a simple linear receiver [41]. In the earliest experiments of this approach regenerative operation of a 3.3 m switch was reported with a pulse operating power of 16 W [39].

It is also possible to extend the spectral broadening followed by offset narrowband filtering technique to work using *cross-phase modulation* (XPM) and thereby to allow for signal wavelength conversion [42]. In this instance a continuous wave probe beam, or indeed multiple probe beams, are launched into the holey fibre along with the data signal. XPM between the control signal and the CW beams results in chirping of the CW laser beam where these beams overlap temporally within the fibre. This frequency chirping can then be converted to a frequency converted signal by passing this chirped signal through a narrowband filter to eliminate the residual unchirped CW signal and the original data signal. In Fig. 4 we show the results of an experiment in which 3 CW probe beams are propagated with a relatively intense 10 Gbit/s RZ-data signal (2.5 ps data pulses) within just 6 m of high nonlinearity HF ($\gamma = 31\ \mathrm{W^{-1}\cdot km^{-1}}$) resulting in the generation of 3 wavelength converted signals over the C-band [43]. Fig. 4 also shows the measured temporal width of the wavelength-converted pulses as a function of probe beam wavelength. The pulse widths of the converted pulses are observed to be almost constant at $\sim$5.8 ps over a wavelength range of $\sim$20 nm. This operation range was limited solely by the tuning range of the tuneable filter since the walk-off effect between control and probe light was negligible due to the short length of HF used. The time-bandwidth product of the converted pulses was $\sim$0.46, indicating the formation of high quality pulses. Note that in order to get the most stable operation of the filtered SPM and XPM schemes described above it is best to use holey fibres with normal rather than anomalous dispersion since coherence degradation is known to result in amplitude noise when anomalously dispersive fibre is used [31]. Fortunately, the combination of high nonlinearity and normal dispersion can readily be achieved using holey fibre technology.

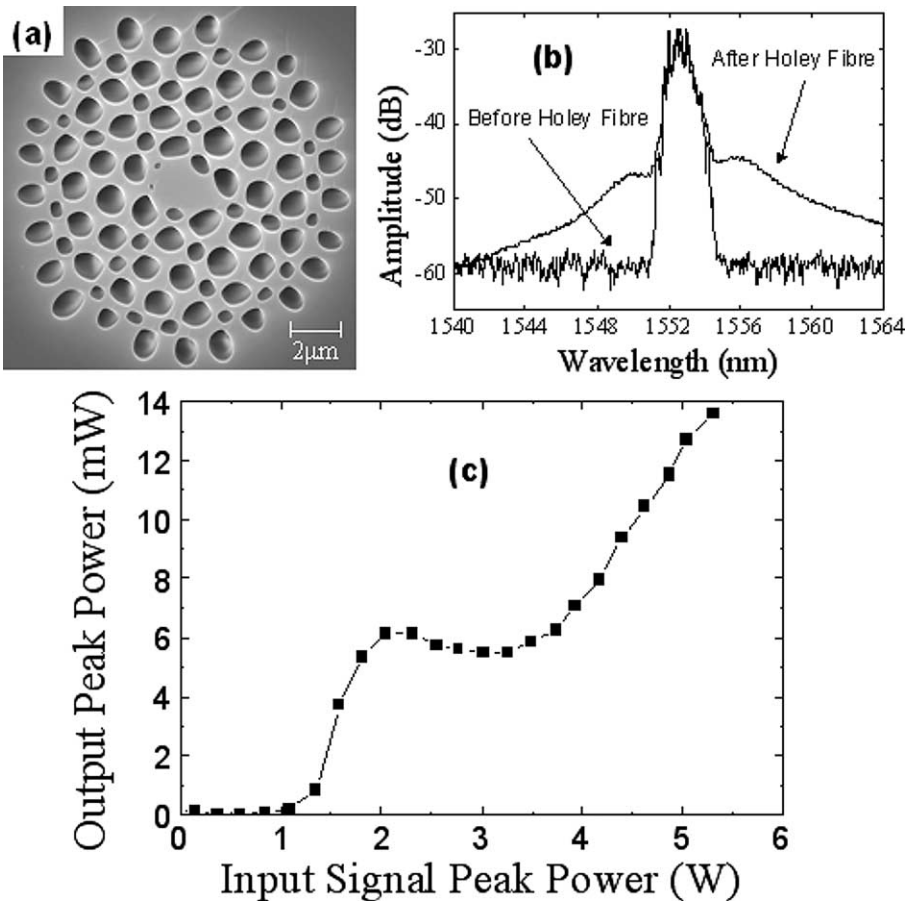


Fig. 3. (a) SEM of small-core HF used for 2*R* regeneration. (b) SPM broadened spectra. (c) Nonlinear transmission characteristic.

An alternative, and more flexible approach for frequency conversion, is based on four-wave mixing (FWM). FWM is particularly attractive for wavelength conversion due to its relative transparency to both bit-rate and modulation format [44]. Highly efficient, broadband wavelength conversion based on FWM in optical fibre requires high nonlinearity, a low value of dispersion, a low dispersion slope, and a short fibre length to reduce the phase mismatch between the interacting waves [45]. The reduction of *stimulated Brillouin scattering* (SBS) effects is also critical in order to suppress SBS induced pump power loss. Holey fibre is of great potential interest for this application since it is possible to produce fibres with a high Kerr nonlinearity, high SBS threshold and low normal dispersion such that a relatively broad device bandwidth with good conversion efficiency can be achieved. The high SBS threshold is obtained by varying the holey fibre structure along the fibre length so as to broaden the Brillouin gain bandwidth [46].

The results of a 10 Gbit/s NRZ four-wave mixing based wavelength conversion experiment employing a 15 m length of holey are shown in Fig. 5. An SEM of the holey fibre used is shown inset. The measured nonlinearity coefficient $\gamma$ of the fibre is $\sim 60 \pm 10\ \mathrm{W}^{-1}\cdot\mathrm{km}^{-1}$ and the measured group velocity dispersion (GVD) was $\sim -30$ ps/nm/km at a wavelength of 1550 nm. Due to structural variation along the fibre length the Brillouin linewidth of the fibre was approximately 50 MHz, two to three times broader than would be expected for a longitudinally uniform silica fibre. The SBS threshold was measured to be $\sim$120 mW and which was well above the power level required to get efficient four wave mixing. The HF output spectrum at the end of the fibre is shown in Fig. 5 (upper). A strong FWM wavelength converted signal is clearly evident at a wavelength of $\sim$1544 nm despite the short fibre length used, and second and third order idler beams are also even observable. After the HF we used a compression tuneable, apodized fibre Bragg grating (FBG) filter to suppress the input signal and pump beam and to pick out the wavelength converted signal. Fig. 5 (lower) shows the measured conversion efficiency, which is defined as the ratio of output wavelength-converted signal power to the input signal power. A maximum conversion efficiency of $-16$ dB was achieved over a 3 dB bandwidth of $\sim$10 nm (further details can be found in [25]).

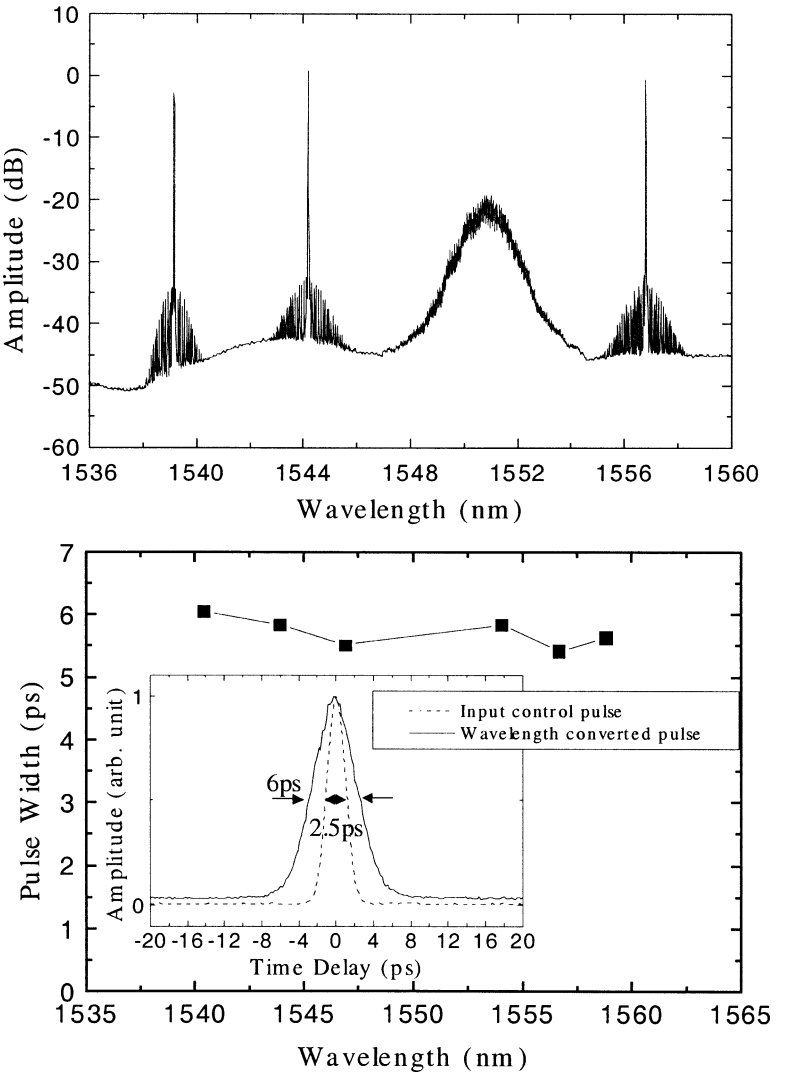


Fig. 4. (Upper) Measured optical spectra of control and probe signals after the HF in a 3 channel XPM experiment. (Lower) Measured FWHM of wavelength converted pulses as a function of probe beam wavelength. Inset: SHG autocorrelation traces of wavelength converted pulses at 1540 nm.

Although the previous device examples made use of the elastic third order Kerr nonlinearity, it worth noting that the tight mode confinement/unusual dispersion effects can also be used to similarly good effect to enhance the performance of fibre devices based on other fibre nonlinearities. For example, poled HF devices based on second order effects should be possible with conversion efficiencies and operating bandwidth two orders of magnitude greater than can be achieved with standard fibres [47]. Similarly, it should be possible to make HF Raman and Brillouin devices with greatly reduced operating powers or device lengths and indeed first experiments in this area have been performed [46,48,49].

Using a fibre similar to that shown in Fig. 3, a HF Raman amplifier was demonstrated. The 75 m long amplifier was configured for co-propagating pump and signal and was pumped using a diode seeded EDFA MOPA. The signal light was generated from a continuous wave external cavity laser tunable in the range 1600–1640 nm. The maximum peak pump power that we could launch into the HF was ∼6.7 W, and the maximum launched signal power was ∼0 dBm. The loss of this fibre and nonlinear coefficient were measured to be 40 dB/km and $\gamma = 32\ \mathrm{W}^{-1}\cdot\mathrm{km}^{-1}$ respectively. The 75 m of HF thus has an effective nonlinear length $L_{\mathrm{eff}}$ of just 54 m. Fig. 6(a) shows internal Raman gain and noise figure for various probe signal wavelengths and fixed pump/signal powers. Higher gains and lower noise figure are observed as the probe signal wavelength approaches the peak of the Raman gain curve around 1650 nm, corresponding to the peak Raman shift of 13.2 THz (Fig. 6(b)). Small signal gains as large as 42.8 dB, and noise figures as low as 6 dB were obtained at 1640 nm. The observed variation in gain with

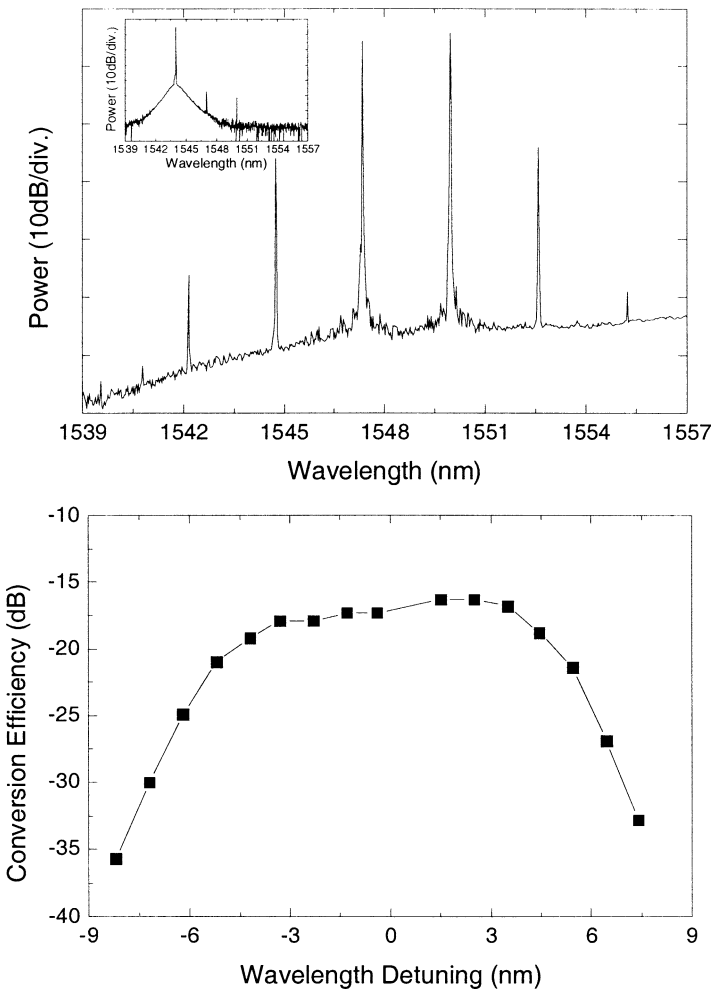


Fig. 5. Four wave mixing wavelength converter: (Upper) Wavelength converted signal (∼1545 nm), pump (∼1552 nm), input signal (∼1549 nm) and idler with filtered spectrum shown inset. (Lower) Conversion efficiency as a function of signal: pump wavelength separation with inset SEM of fibre cross section.

wavelength was in good agreement with our expectations based on published data on the Raman lineshape of silica. As well as investigating the performance of the HF as a pure Raman amplifier we also performed a Raman modulator/erasure experiment and extinction ratios in excess of ∼11 dB were obtained for peak powers of ∼5 W and above.

## 6. Active holey fibres

Although research on holey fibres has concentrated largely on single-material designs, it straightforward to extend capillary stacking fabrication techniques to allow the production of doped fibres, and many of the properties of HFs have benefits for active devices. HFs incorporating $Er^{3+}$ [50] and $Yb^{3+}$ have been fabricated, and CW [51] and mode-locked [52] $Yb^{3+}$ HF lasers have been realised. HFs with anomalous dispersion extending down through the visible regions of the spectrum opens the prospect of extending soliton laser techniques that have been developed for 1550 nm, to $Yb^{3+}$ doped and $Nd^{3+}$ doped fibre lasers. Here we review two demonstrations of active devices based on $Yb^{3+}$-doped holey fibres: (a) a tunable fs-soliton source based on highly nonlinear HF; and (b) a cladding pumped laser based on double clad large mode area HF.

### *6.1. Tunable fs-soliton source*

Wavelength tuneable femtosecond (fs) pulse sources have applications in areas including ultrafast spectroscopy, materials processing and nonlinear optics. Traditional fs pulse sources based on bulk crystals offer a limited wavelength range, particularly

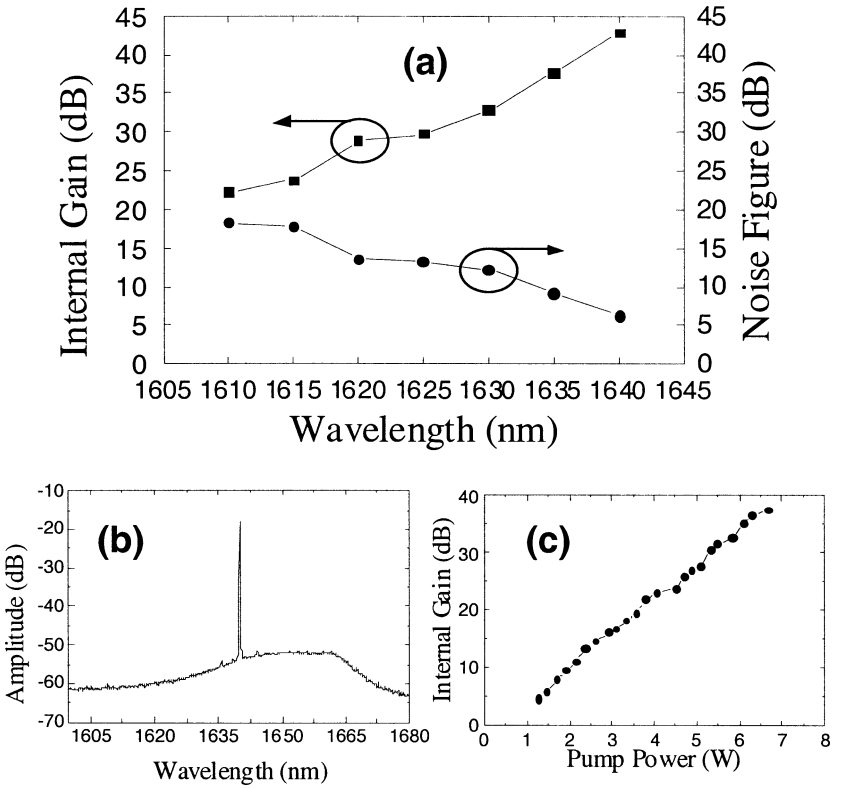


Fig. 6. Raman amplifier: (a) Internal Raman gain and noise figure for various probe signal wavelengths (signal power: −10 dBm, pump peak power: 6.7 W). (b) Typical (high gain) amplifier spectrum showing Raman ASE spectrum. (c) Internal gain versus pump power at 1635 nm.

above 1.1 μm. The discovery of the *soliton-self-frequency shift* (SSFS) in fibres [53] has opened up the possibility of wavelength tuneable fs soliton fibre sources. To use the SSFS effect, the frequency shifting fibre must exhibit anomalous dispersion at the seed wavelength and across the required tuning range. Although conventional fibres can have anomalous dispersion beyond 1.3 μm, small core, large air filling fraction HFs extend this range down to 550 nm [9]. Such fibres have a high effective nonlinearity, which allows soliton formation with just pJ pulse energies in meter long fibre lengths [54].

Here we describe a continuously tuneable soliton source operating from 1.06–1.33 μm based on HF technology. A fuller exposition of this work can be found in [28]. This source is seeded by a diode-pumped 1.06 μm $Yb^{3+}$-doped silica fibre laser, and relies upon SSFS effects in an $Yb^{3+}$-doped holey fibre amplifier. The fibre used in these experiments is shown in Fig. 1 (right). This fibre is single mode for all wavelengths considered here, and has an effective mode area of just $A_{\text{eff}} \approx 2.5\ \mu m^2$ at 1.55 μm.

The mode-locked seed laser produces pulses at 1.06 μm with a positive linear chirp, which are launched into $Yb^{3+}$-doped HF amplifier, together with a pump beam from a diode laser to control the gain. Because of the amplification and nonlinear evolution of the pulses as they pass through the amplifier, Raman solitons form and are continuously wavelength shifted via the SSFS. Since the nonlinear evolution of the pulses depends on the pulse peak power, the wavelength of the Raman solitons at the amplifier output can be tuned by varying the gain in the amplifier. Using ∼5 m of amplifier fibre, monocolour soliton output pulses have been wavelength tuned from 1.06–1.33 μm. At higher pump powers the change in gain distribution causes the Raman solitons to form earlier within the amplifier, thereby leaving them a greater length of fibre within which to walk-off to longer wavelengths through the SSFS. The final central wavelength of the pulses varies in an almost linear fashion with the level of incident pump power. Note that the maximum wavelength shift of the Raman soliton increases with the length of fibre used, and is ultimately limited by the absorption of silica near 2.3 μm [55].

### *6.2. Cladding pumped fibre laser*

The preforms for the *large mode area* (LMA) HFs described in Section 5, like most holey fibres, are produced using capillary stacking techniques. It is straightforward to extend this approach to allow the production of all-glass double-clad fibres, and an example is shown in Fig. 2 (right). The approach is attractive for high power active fibre devices, because it allows the use of

cladding pumping, and here we review some recent laser demonstrations based on double-clad HF (a detailed description can be found in [55]). The fibre in Fig. 2 (right) has an $Yb^{3+}$-doped core surrounded by an inner cladding consisting of 5 rings of small ($d \approx 2.7$ μm) holes separated by $\Lambda \approx 9.7$ μm. The inner cladding NA was measured to be 0.3 in a ∼10 cm fibre length. Two rings of larger holes define the outer cladding. Note that the core is offset, which breaks the cladding symmetry, and hence enhances the pump absorption.

A Ti:Sapphire pump laser operating at 976 nm was used to examine the laser performance of the fibre. The free-space pump coupling efficiency was ∼70%, and the laser cavity was formed by the ∼4% Fresnel reflection from the launch end and a high reflector placed at the other end of the fibre. Slope efficiencies as high as 82% were recorded in a 4 m fibre length, comparable to the best conventional ytterbium fibre lasers. As expected, the output beam was robustly single-mode. Due to the low NA of the inner core/cladding structure, a significant fraction of the pump was launched into the inner cladding, and so this laser acts as a hybrid core/cladding pumped fibre laser.

A cladding pumped laser was realized using a low brightness 915 nm fibre-coupled laser diode. Again using a Fabry-Perot cavity, average powers in excess of 1 W were achieved in 7.5 m fibre length, with a measured slope efficiency of 70%. Note that in addition to optically isolating the inner structure from the external environment, the air cladding also provides thermal isolation. Although this might be expected to lead to thermal problems, no such issues were encountered in these experiments even at multi-Watt pump levels.

Furthermore, both Q-switched and mode-locked operation were demonstrated in this cladding-pumped HF laser. In the mode-locking experiments, fundamental modelocking was obtained over a wavelength tuning range in excess of 60 nm. The pulse duration was estimated to ∼100 ps. An output power of more than 500 mW was achieved for a pump power of 1.33 W. Ultimately, it should be possible to develop compact ∼multi 10 nJ femtosecond pulse sources operating at 1 μm using LMA HF.

The ultimate advantages of these fibres relative to polymer coated dual clad fibres are that they allow for all-glass structures, with inner cladding NAs in excess of 0.5 and good pump/mode mixing. In addition, they offer the combination of single-mode guidance and large core dimensions. In device terms, these features translate to the possibility of higher coupled diode powers, shorter device lengths and extended tuning ranges.

## 7. Conclusion

The field of holey optical fibres has developed rapidly, and a wide range of robust, low loss index-guiding HFs can now routinely be fabricated. The novel guidance regimes that have been identified in these fibres promise to lead to a new generation of optical devices with tailor-made optical properties. One of the objectives of this paper has been to describe a range of recent research results that exploit the unique features of holey fibres. One area in which significant progress has been made recently is the field of highly nonlinear index-guiding holey fibres, and recent developments in this area include optical data regeneration, wavelength conversion, generation of supercontinuum spectra, and a range of new source and amplifier technologies. As holey fibre technology becomes increasingly mature, it seems likely that the many unique features of these fibres will lead to numerous applications within telecommunications and beyond.

## Acknowledgements

The authors would like to thank colleagues at the ORC, University of Southampton, for contributions to the research presented here. Warm thanks to Kentaro Furusawa, Vittoria Finazzi, Joanne Baggett, Periklis Petropoulous, Walter Belardi, Ju Han Lee and Jonathan Price. The authors acknowledge the support of a Royal Society University Research Fellowships.

## References

[1] T.A. Birks, P.J. Roberts, P.St.J. Russell, D.M. Atkin, T.J. Shepherd, Electron. Lett. 31 (1995) 1941.
[2] T.M. Monro, Y.D. West, D.W. Hewak, N.G.R. Broderick, D.J. Richardson, Electron. Lett. 36 (2000) 1998–2000.
[3] M. van Eijkelenborg, M. Large, A. Argyros, J. Zagari, S. Manos, N.A. Issa, I.M. Bassett, S.C. Fleming, R.C. McPhedran, C.M. deSterke, N.A.C. Nicorovici, Opt. Express 9 (2001) 319–327.
[4] T.M. Monro, P.J. Bennett, N.G.R. Broderick, D.J. Richardson, Opt. Lett. 25 (2000) 206–208.
[5] T.M. Monro, D.J. Richardson, N.G.R. Broderick, P.J. Bennett, IEEE J. Lightwave Technol. 17 (1999) 1093–1101.
[6] N.G.R. Broderick, T.M. Monro, P.J. Bennett, D.J. Richardson, Opt. Lett. 24 (1999) 1395–1397.
[7] J.C. Knight, T.A. Birks, R.F. Cregan, P.St.J. Russell, J.-P. DeSandro, Large mode area photonic crystal fibre, Electron. Lett. 34 (1998) 1347–1348.
[8] T.A. Birks, J.C. Knight, P.St.J. Russell, Opt. Lett. 22 (1997) 961–963.

[9] J.C. Knight, J. Arriaga, T.A. Birks, A. Ortigosa-Blanch, J.W. Wadsworth, P.St.J. Russell, IEEE Photonics Technol. Lett. 12 (2000) 807–809.
[10] R.F. Cregan, B.J. Mangan, J.C. Knight, T.A. Birks, P.St.J. Russell, P.J. Roberts, D.C. Allan, Science 285 (1999) 1537–1539.
[11] J. Broeng, T. Søndergaard, S. Barkou, P. Barbeito, A. Bjarklev, Pure Appl. Opt. 1 (1999) 477–482.
[12] J.C. Knight, T.A. Birks, P.St.J. Russell, D.M. Atkin, Opt. Lett. 19 (1996) 1547–1549.
[13] R.T. Bise, R.S. Windeler, K.S. Kranz, C. Kerbage, B.J. Eggleton, D.J. Trevor, in: Proc. Conference of Optical Fiber Communications, OFC '2002, OSA Technical Digest, Anaheim, CA, 2002, pp. 466–467, paper xxx.
[14] K.M. Kiang, K. Frampton, T.M. Monro, R. Moore, J. Tucknott, D.W. Hewak, D.J. Richardson, Electron. Lett. 38 (2002) 546–547.
[15] J. Riishede, S.B. Libori, A. Bjarklev, J. Broeng, E. Knudsen, in: Proc. 27th European Conference on Optical Communication ECOC '2001, Amsterdam, 2001, p. xxx, paper Th.A. 1.5.
[16] B.J. Eggleton, P.S. Westbrook, R.S. Windeler, S. Spalter, T.A. Strasser, Opt. Lett. 24 (1999) 1460–1462.
[17] F. Brechet, J. Marcou, D. Pagnoux, P. Roy, Opt. Fiber Technol. 6 (2000) 181–191.
[18] J. Broeng, D. Mogilevstev, S.E. Barkou, A. Bjarklev, Opt. Fiber Technol. 5 (1999) 305–330.
[19] T.M. Monro, D.J. Richardson, N.G.R. Broderick, P.J. Bennett, IEEE J. Lightwave Technol. 18 (2000) 50–56;
T.M. Monro, N.G.R. Broderick, D.J. Richardson, in: NATO Summer School on Nanoscale Linear and Nonlinear Optics, Erice, Sicily, 2000.
[20] M.J. Steel, T.P. White, C.M. deSterke, R.C. McPhedran, L.C. Botten, Opt. Lett. 26 (2001) 488–490.
[21] T.P. White, R.C. McPhedran, C.M. deSterke, L.C. Botten, M.C. Steel, Opt. Lett. 2 (2001) 1660–1662.
[22] L. Poladian, N.A. Issa, T.M. Monro, Opt. Express 10 (2002) 449–454.
[23] G.P. Agrawal, Nonlinear Fiber Optics, Academic Press, New York, 1989.
[24] T. Okuno, M. Onishi, T. Kashiwada, S. Ishikawa, M. Nishimura, IEEE J. Sel. Top. Quant. Electron. 5 (1999) 1385–1391.
[25] W. Belardi, J.H. Lee, K. Furusawa, Z. Yusoff, P. Petropoulos, M. Ibsen, T.M. Monro, D.J. Richardson, in: Proc. European Conference on Optical Communications, ECOC '02, Copenhagen, Denmark, 2002, paper PD1.2.
[26] L. Farr, J.C. Knight, B.J. Mangan, P.J. Roberts, in: Proc. European Conference on Optical Communications, ECOC '02, Copenhagen, Denmark, 2002, paper PD1.3.
[27] V. Finazzi, T.M. Monro, D.J. Richardson, in: Proc. Conference on Optical Communications, OFC '2002, OSA Technical Digest, Anaheim, CA, 2002, pp. 524–525.
[28] J.H.V. Price, K. Furusawa, T.M. Monro, L. Lefort, D.J. Richardson, J. Opt. Soc. Am. B 19 (2002) 1286–1294.
[29] J.K. Ranka, R.S. Windeler, A.J. Stentz, Opt. Lett. 25 (2000) 25–27.
[30] T.A. Birks, D. Mogilevtsev, J.C. Knight, P.St.J. Russell, IEEE Photonics Technol. Lett. 11 (1999) 674–676.
[31] N. Nakazawa, H. Kubota, K. Tamura, Opt. Lett. 24 (1999) 318–320.
[32] M. Asobe, Opt. Fiber Technol. 3 (1997) 142–148.
[33] S.R. Friberg, P.W. Smith, IEEE J. Quantum Electron. 23 (1987) 2089–2094.
[34] J.C. Baggett, T.M. Monro, K. Furusawa, D.J. Richardson, Opt. Lett. 26 (2001) 1045–1047.
[35] A. Gambling, et al., Microwaves Opt. Acoust. 2 (1978) 134–140.
[36] T. Sorensen, J. Broeng, A. Bjarklev, E. Knudsen, S.E. Barkou Libori, Electron. Lett. 37 (2001) 287.
[37] J.C. Baggett, T.M. Monro, K. Furusawa, D.J. Richardson, in: Proc. Conference on Lasers and Electro-Optics, CLEO 2002, Long Beach, CA, Optical Society of America, 2002, paper CMJ6.
[38] D. Marcuse, Appl. Opt. 21 (1982) 4208–4213.
[39] P. Petropoulos, T.M. Monro, W. Belardi, K. Furusawa, J.H. Lee, D.J. Richardson, Opt. Lett. 26 (2001) 1233–1235.
[40] P.V. Mamyshev, in: Proc. European Conference on Optical Communications, ECOC '98, Madrid, 1998, p. 475.
[41] J.H. Lee, J. Teh, Z. Yusoff, W. Belardi, M. Ibsen, T.M. Monro, D.J. Richardson, IEEE Photonics Technol. Lett. 14 (8) (2002) 876–878.
[42] P. Ohlen, B.E. Olsson, D. Blumenthal, IEEE Photonics Technol. Lett. 12 (2000) 522–524.
[43] J.H. Lee, Z. Yusoff, W. Belardi, M. Ibsen, T.M. Monro, B. Thomsen, D.J. Richardson, in: Proc. Conference on Lasers and Electro-Optics, CLEO '2002, Long Beach, 2002, postdeadline CPDB5.
[44] K. Inoue, H. Toba, IEEE Photonics Technol. Lett. 4 (1992) 69–72.
[45] O. Aso, S. Arai, T. Yagi, M. Tadakuma, Y. Suzuki, S. Namiki, Electron. Lett. 36 (2000) 709–711.
[46] J.H. Lee, Z. Yusoff, W. Belardi, M. Ibsen, T.M. Monro, B. Thomsen, D.J. Richardson, Opt. Lett. 27 (2002) 927–929.
[47] T.M. Monro, V. Pruneri, N.G.R. Broderick, D.J. Richardson, IEEE Photonics Technol. Lett. 13 (2001) 981–983.
[48] Z. Yusoff, J.H. Lee, W. Belardi, T.M. Monro, P.C. Teh, D.J. Richardson, Opt. Lett. 27 (2002) 424–426.
[49] J. Nilsson, R. Selvas, W. Belardi, J.H. Lee, Z. Yusoff, T.M. Monro, D.J. Richardson, K.D. Park, P.H. Kim, N. Park, in: Proc. Optical Fiber Communications, OFC '2002, Anaheim, 2002.
[50] R.F. Cregan, J.C. Knight, P.St.J. Russell, P.J. Roberts, IEEE J. Lightwave Technol. 17 (1999) 2138–2141.
[51] W.J. Wadsworth, J.C. Knight, W.H. Reeves, P.St.J. Russell, J. Arriaga, Electron. Lett. 36 (2000) 1452–1454.
[52] K. Furusawa, T.M. Monro, P. Petropoulos, D.J. Richardson, Electron. Lett. 37 (2001) 560–561;
F.M. Mitschke, L.F. Mollenauer, Opt. Lett. 11 (1986) 659–661.
[53] J.H. Price, W. Belardi, L. Lefort, T.M. Monro, D.J. Richardson, in: Proc. Nonlinear Guided Waves and Their Applications, NLGW 2001, 2001, paper WB1-2.
[54] M.E. Fermann, A. Galvanauskas, M.L. Stock, K.K. Wong, D. Harter, L. Goldberg, Opt. Lett. 24 (1999) 1428–1430.
[55] K. Furusawa, A.N. Malinowski, J.H.V. Price, T.M. Monro, J.K. Sahu, J. Nilsson, D.J. Richardson, Opt. Express 9 (2001) 714–720.